Journal of Energy Storage 72 (2023) 108422

Contents lists available at ScienceDirect

Journal of Energy Storage

journal homepage: www.elsevier.com/locate/est

Research papers

Investigation of constant stack pressure on lithium-ion battery performance

Aiden Leonard *, Brady Planden, Katie Lukow, Denise Morrey

High Voltage Energy Storage Group, School of Engineering, Computing, and Mathematics, Oxford Brookes University, Oxford, OX33 1HX, UK

ARTICLE INFO

Dataset link: https://www.brookes.ac.uk/research/units/tde/groups/high-voltage-and-energy-storage

Keywords:
Lithium-ion battery
Pack design
Stack pressure
Battery performance

ABSTRACT

Current research involving applying stack pressure to lithium-pouch cells has shown both performance and lifetime benefits. Fixtures are used to mimic this at the cell level and conventionally prescribe a constant displacement onto the cell. This increases stack pressure, but also causes pressure to vary. Despite this, applying an initial stack pressure improves cell conductivity and cell lifetime (Mussa et al., 2018, Zhou et al., 2020, Müller et al., 2019, Li et al., 2022, and Cannarella and Arnold, 2014). In this work, a fixture was designed that applies constant pressure to the cell independent of displacement. The fixture uses pneumatics to apply a constant stack pressure independent of elastic and plastic swelling. Cells constrained by the constant pressure fixture and a conventional displacement based fixture were evaluated using a Hybrid Pulse Power Characterisation (HPPC) test to measure internal resistance and maximum deliverable power. Multiple stack pressures were applied to investigate the variance in pressure over operational conditions and performance between constant pressure and constant displacement based methods. All tests were further compared to a control case with no applied stack pressure. The constant pressure based method reduced pressure variation during charging and discharging, reduced the discharge impedance and improved discharged power, but did not improve charge performance. Discharge performance benefits from constant pressure could influence pack design to improve vehicle performance.

1. Introduction

Lithium-ion cells have quickly become the standard for many industries requiring reliable and efficient battery storage. Pouch cells provide a unique solution for increased packaging density and increased power density when compared to most conventional cylindrical cells; however, they bring additional challenges as well. Most notably, is the requirement of external stack pressure to prolong life and optimise performance. Stack pressure has been applied to pouch cells via various methods, generally falling into two categories, fixed displacement and constant pressure. Conventionally, fixed displacement is achieved by constraining the orthonormal expansion of the cell through rigid plates. Constant pressure based methods conventionally allow for expansions of the cell through the additions of varying-stiffness foam or spring elements [1,2]. Pressure has been shown to improve the interfacial surface area between the negative electrode, positive electrode, and separator, thus decreasing the ionic resistivity [3–6]; however, reaches a critical value where additional mechanical stress has been shown to reduce active electrode material, reducing the performance of cells [5–8]. Stack pressure varies elastically throughout the battery's state-of-charge for a corresponding fixed displacement fixture due to lithiation of the anode and increases over time due to anode growth [1,9–12]. Development of a stack pressure method that is cell thickness agnostic is the aim of this work, potentially providing performance benefits through increasing the positive effects of pressure without causing damage through uncontrolled pressure increases due to ageing [1].

Current research involving applying stack pressure to pouch cells has resulted in immediate and long-term performance benefits. A study conducted by Müller et al. [5] utilised parallel plates with springs to apply pressure ranging from 0–0.84 MPa to both a full NMC/graphite cell and the individual cathode, anode, and separator. The results show an optimal pressure to minimise separator resistivity from 0.1–0.6 MPa, and an increasing relationship between the electrode resistances and pressure. At the cell level, stack pressure increased the charge transfer resistance but decreased the high frequency resistance. Pressures above 100 kPa have been seen to improve conductivity for future cell materials, such as lithium-metal and solid electrolytes [13–15]. Doux et al. [13] explored the effect of stack pressure on a sulfide electrolyte solid-state battery and tested pressures from 5 MPa to 70 MPa. Electrode conductivity improved for pressures up to 70 MPa, while discharge capacity decreased at the upper limit of pressure tested. A study conducted by Louli et al. [16] found that 1.7 MPa of stack pressure provided the highest performance for a lithium-metal negative electrode cell using a liquid electrolyte; However, the study reported a

* Corresponding author.
E-mail address: atleonard97@gmail.com (A. Leonard).

https://doi.org/10.1016/j.est.2023.108422
Received 12 January 2023; Received in revised form 5 July 2023; Accepted 16 July 2023
Available online 31 July 2023

Abbreviations

Symbol	Definition
CPF	Constant pressure fixture
DCIR	Direct current internal resistance
D_{max}	100% Maximum discharge current
$D_{max/2}$	50% Maximum discharge current
HPPC	Hybrid pulse power characterisation
MBPF	Modular battery pressure fixture

50%–300% change in pressure from the thickness change of the cell during charging and discharging. A hybrid lithium-ion/lithium-metal cell was also found to benefit from 1.2 MPa of applied stack pressure, [17] enabling a dendrite suppression mechanism which corresponds to cycle-life benefits. For lithium-ion cells, the SEI layer has been shown to grow over the life of the cell, increasing impedance and decreasing usable capacity [18]. Stack pressure is shown to reduce capacity fade through suppressing delamination of electrodes, gassing of the electrolyte, and SEI layer growth [7,11]. Hahn et al. [1] presents a varying applied stack pressure between 38-580 kPa, improved capacity retention from 95% to 99% after 70 days of calendar ageing. Further studies support the discharge capacity improvement gained from reducing the applied current density due to pressure application [19,20]. Along with capacity improvements, increasing stack pressure for lithium-ion cells has shown to improve interfacial contact of electrodes to the separator [7]. Since non-flat electrode surfaces have a limited contact surface area, creating a more ideal flat surface contact between elements in cells results in immediate performance benefits. With elastic contact on rough surfaces, the contact area increases proportionally to the load [21–23]. Improving interfacial surface area contact immediately reduces the current density in the localised region [20]. The larger interaction area between electrodes also reduces the effective ion path length, further reducing impedance [15]. These performance benefits from applying a stack pressure influence current and next-generation battery pack design. Current modules have two main methods of applying stack pressure. Modules fix the outer dimensions of cells using cylindrical cells or volumetrically constricted groups of pouch cells [24]. Furthermore, deformable materials are used between cells to reduce pressure variance from expansion and contraction [1]. Based on current research on lithium-metal [14,17] and Silicon [13,19,25] cells, future battery packs will likely benefit from higher stack pressure applied to cells. Studies look for performance benefits by either constraining thickness or using spring-like elements.

Basic fixtures use flat parallel plates and apply pressure by using bolt torques to clamp the cell between the plates [13,26,27]. However, because the width between each plate is essentially fixed, stack pressure varies during charging and discharging due to elastic swelling, with SOC due to differences in electrode volumes, and over time increases due to negative electrode growth [1,28–30]. Hahn et al. [1] studied the long-term effects of mechanical pressure by using a hydraulic cylinder and porous foam as a spring element. This approach provided flexibility in altering pressure to model cell elasticity as a spring-like element; however, this study did not observe the effects of constant pressure due to the pressure increase over cell lifetime corresponding with cell thickness growth. Other novel fixtures [2,17], utilise buffer layers of foam to dampen the thickness growth; however, stack pressure then becomes dependent on the compressive stiffness of the foam. Conventionally, to apply a constant, high amplitude pressure, three methods are utilised: electric, hydraulic, or pneumatic actuation. Using pneumatic actuation has conventionally provided advantages of low viscosity and compressibility, thus minimising the pressure variance to a corresponding volume change; however, a system leakage is common causing the need for an air compressor. Hydraulic actuation commonly provides the lowest cost with minimal leakage under normal operation; however, even minimal hydraulic leaks could cause an electrical short circuit for the tested battery. Electric actuation can provide a constant pressure over long periods, but the corresponding high power consumption and pressure dependency on motor and sensor accuracy are not ideal. Due to the above limitations, hydraulic and electric actuation were ruled out due to the risk of short circuits and high costs. As pneumatic actuation does not suffer from these limitations and has a relatively low cost, it was selected for this work.

The performance impacts of constant pressure on lithium-ion pouch cell is relatively unknown. As previously discussed, constant pressure research has been previously focused on low amplitude (<40 N Jiang et al. [2]) or amplitudes above 1 MPa for lithium-metal chemistries [14]. In this paper, a constant pressure fixture (CPF) utilising pneumatic actuation for stable pressure values independent of elastic and plastic swelling is presented.

2. Methodology

The following section provides an overview of the fixture design, data acquisition and analysis methods, and experimental methods.

2.1. Fixture design

A novel fixture was designed to maintain a constant face pressure during cell cycling using a pneumatic actuator. The design targeted up to 180 kPa for testing current-generation liquid electrolyte cells with the ability to replace the pneumatic actuator to allow for larger face pressures if required. Fig. 1 presents the design of the proposed constant pressure fixture (CPF) and the reference constant displacement fixture, referred to as the modular battery pressure fixture (MBPF). The fixture applies a constant stack pressure to the face of the battery through the pneumatic actuator and is transferred through two carbon-inlaid 3D-printed plates. This material electrically isolates the battery to prevent the risk of short circuits and provides sufficient stiffness to improve pressure distribution. The ball-and-socket joint provides rotational freedom, allowing the contact between the cell and the pressure plates to be uniform and less dependent cell swelling. Two TE FX29 load cells measure force, that are monitored through a Teensy 4.1 board and recorded onto a microSD card.

Results in this work were compared against two other fixture methods. A baseline condition of no external stack pressure was first tested. Second, a constant displacement fixture developed by the High Voltage and Energy Storage group as shown in Fig. 1 [31]. The fixture applies stack pressure through two plates fastened at up to 6 locations, measured through TE FX29 sensors similar to the constant pressure fixture. Further information can be found in the GitHub repository. As discussed, stack pressure was applied through a pneumatic piston connected to an air reservoir to counteract cell swell and minor leaks within the system. Initial testing showed that pressure was maintained over a 48 h period (see Fig. 2).

Two TE FX29 load cells were placed between the lower cell plate and the base of the test fixture. The load cells were connected to a Teensy 4.1 microcontroller that recorded the values throughout the test via a microSD card. A type-T thermocouple was placed on the body of the cell located near the cell tabs. An Arbin LBT-21084-HC cell cycler was used to perform the experiments.

2.2. Test method

A 3.7 Ah LCO/graphite pouch cell was used throughout this study with specifications as defined in Table 1.

A Hybrid Pulse Power Characterisation (HPPC) test was conducted every 5% state-of-charge, beginning at 100% SOC. A pulse profile a 10 s load followed by a 40 s rest was completed as shown in Fig. 3.

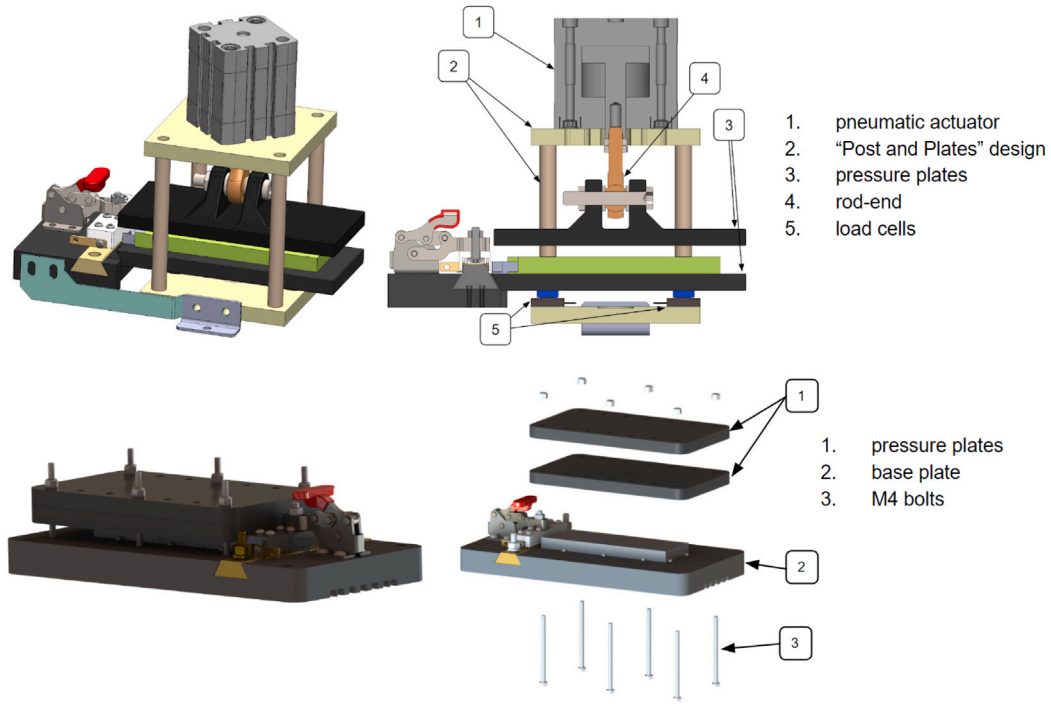

Fig. 1. CPF (top) and MBPF [31] (bottom) CAD, with crucial design elements enumerated.

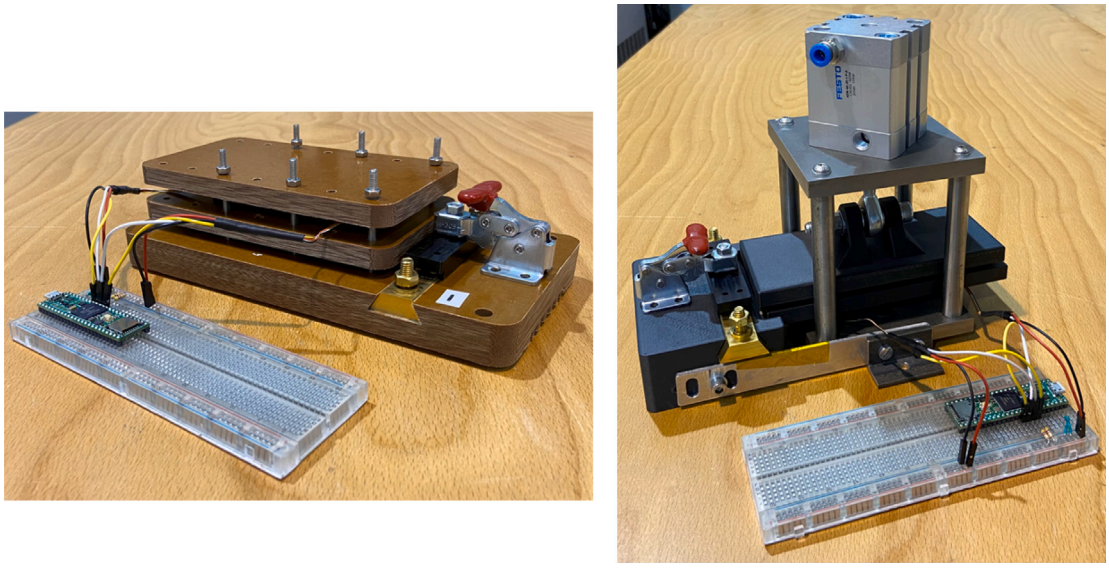

Fig. 2. Test measuring pressure variation over 24 h between the MBPF (left) and CPF (right).

Table 1
Rated cell specifications [32].

Cell	Chemistry	Nominal voltage [V]	Initial AC impedance mΩ	Initial DC resistance mΩ	Nominal capacity [Ah]	Energy density [Wh/kg]	Power density [W/kg]
Melasta SLPB 7336128HV	LCO/NMC	3.8	<2.6	N/A	3.7	204	5043

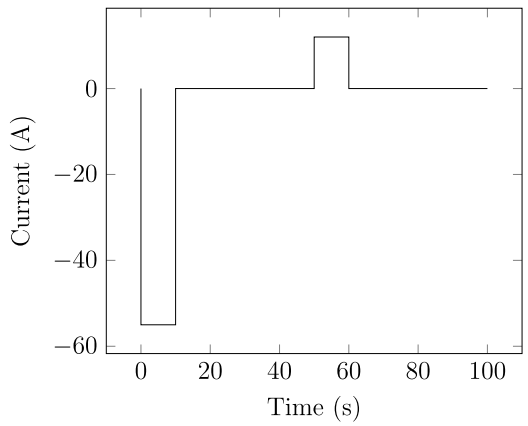

Fig. 3. HPPC pulse profile.

The test was performed at the maximum discharge and maximum charge as shown in the figure above. Tests were also completed at half these values. Stack pressures were compared at 30, 60, and 90 kPa alongside a benchmark test that had no stack pressure applied. Ambient temperature was fixed at 25 °C for all conditions.

3. Results and discussion

3.1. Pressure variance

Pressure data was recorded for all 21 experiments. For all experiments, pressure increased respective to both SOC and pulse current. Pressure varied more with the MBPF over the tests, for 60 kPa of initial stack pressure, the MBPF pressure varied from 44–171 kPa, while the CPF cell pressure varied from 54–69 kPa. The measured stack pressure increased during both the charge and discharge current pulses (Fig. 4). The relationship between pressure and SOC for each pulse (Fig. 5) shows The CPF having a linear slope with an increased slope above 60% SOC; however, the MBPF's fixed displacement method resulted in a large pressure vs SOC slope compared to the CPF. While the MBPF provides poor performance across the full SOC operational range, within 30%–60% it has a small range of potential acceptable usage with a delta of 26.7%–56.7%. The MBPF pressure vs SOC slope was lower for 90 kPa of initial stack pressure at above 80% SOC, compared to 30 kPa and 60 kPa. This could be due to physical deformation of the cell orthogonal to the clamping force, or due to deformation of the MBPF itself. According to Li et al. [6] and Hahn et al. [1], increased cell deformation occurs above 1000 kPa, therefore the most likely cause of the decline in slope of pressure vs SOC is the elastic creep of the MBPF fixture itself. For the MPBF, significant changes in pressure occur at approximately 30% and 60% SOC. This is expected to correspond with the knee points in the open-circuit potential as per Fig. 4, as the thickness of the cell aligns with the voltage vs SOC curve [28].

The CPF provides a reduction in pressure variance and as such improves future pouch cell related pressure independence studies. For example, he MBPF stack pressure increased up to 317% of the initial value for 30 kPa, while the CPF increased by 6%. By utilising the CPF, variance in pressure has been shown to be within +/- 25%, reducing pressure variance disruption on results. Since stack pressure has been shown to affect discharge capacity over cycle life, [3,5,12,17], improved pressure control would enable pressure invariant isolation of these effects. For example, excessive stack pressures can lead to crack development in the electrode active material, with the CPF's ability to adapt to varying thickness this mitigates this mechanism and further provides clarity on the cell lifetime for a given pressure.

Transient pressure variations can occur due to the heat generation occurring inside the cell. Cells produce heat primarily from joule heating, introduced as,

$$Q = I^2 R \tag{1}$$

where I is the current through the cell and R is the internal resistance of the cell [33,34]. As current was applied during the pulses, the cell temperature correspondingly increased. This results in cell swelling [35,36] and therefore pressure should the pouch cell have its displacement constrained. The pressure variance during pulses (Fig. 4) was similar between the MBPF and CPF, although the MBPF did have a higher variance. A reason the CPF may have performed similarly to the MBPF could be its reduced ability to adjust to cell thickness changes in short time frames. Friction between moving and static components may prevent the CPF from adjusting quickly enough to displacement changes to keep stack pressure constant in more transient scenarios. In the case of a battery pack, logging stack pressure to measure transient changes could be useful to gain information on cell energy and heat generation, in addition to temperature management.

Additionally, lithium-ion cell thickness growth over time due to SEI layer growth and reduced packing efficiency further emphasises the importance of the CPF for degradation testing. As the cell thickness increases during ageing, a constant displacement constraint would result in rising pressures over time. This could lead to mechanical damage, chemical degradation, and premature failure due to excessively increasing stack pressures [7,26]. Using a constant pressure constraint would keep pressures more level even as the cell degrades. This would allow for a more accurate degradation analysis for a given pressure. The CPF could provide the capability of conducting degradation testing at various pressures with accurate SOH and failure results. A cycling ageing experiment using the same pressure values and fixtures with a 1C standard charge and discharge could be conducted to compare capacity loss between constant displacement and constant pressure. Following the experiment with a postmortem scanning electron microscope, analysis could reveal any physical and chemical degradation effects on cells from the pressure application method.

3.2. Cell performance

Throughout this study, DC internal resistance was measured through the HPPC pulse and is defined as,

$$R = \frac{V_f - V_0}{I} \tag{2}$$

where V_f is the voltage measured at the end of the 10-second pulse, V_0 is the voltage at the beginning of the pulse and I is the average current applied over the 10-second pulse. A clear difference emerged in both charge and discharge DCIR between the CPF and MBPF while initial pressure varied results for both the CPF and MBPF DCIR. For all initial pressures, the CPF condition generally outperformed the MBPF for both discharge and charge DCIR. Both the CPF and MBPF had the lowest discharge DCIR values at 30 and 60 kPa, while the benefits decreased at 90 kPa. The change in DCIR measured by the CPF and MBPF compared to the control condition with 0 kPa of stack pressure can be seen in Figs. 6 and 7. The CPF and MBPF results are plotted against each other at each initial pressure for both the $D_{\max}$ cycle and the $D_{\max/2}$ cycle. These plots show the difference in DCIR of the CPF and MBPF compared to the control condition, indicated by the dashed line at $y = 0$.

For the discharge pulses (Fig. 6), the CPF had lower DCIR than both the MBPF and control conditions for SOCs below 80%. Above 80% SOC, the CPF only had lower DCIR at 90 kPa initial pressure. The MBPF generally had lower DCIR than the control condition in discharge for $D_{\max/2}$, except for 90 kPa. For $D_{\max}$, the MBPF discharge DCIR was unanimously higher than the control condition. The CPF stands out as having lower discharge DCIR than both the MBPF and

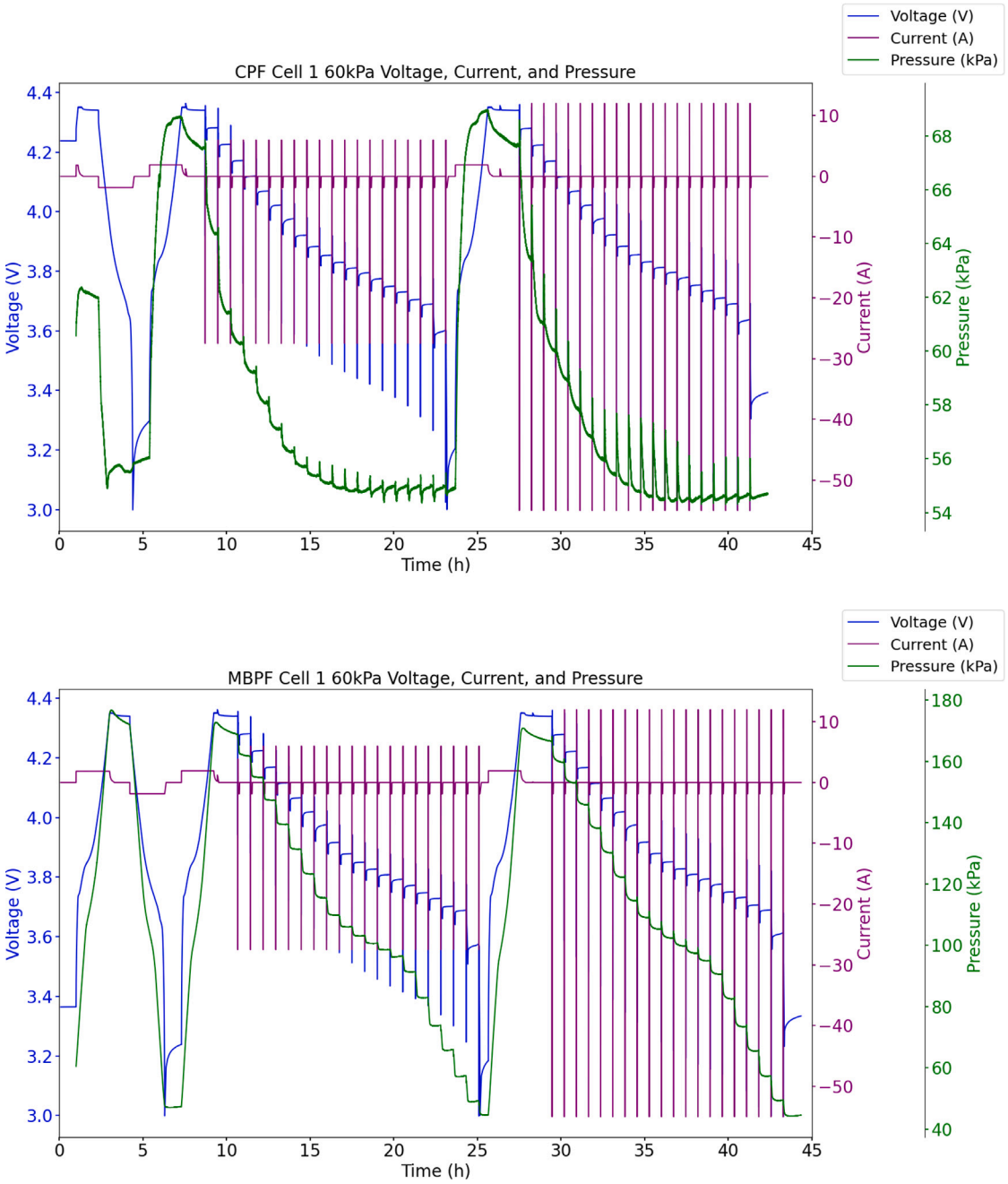

Fig. 4. The pressure, voltage, and current throughout the test for CPF (top) and MBPF (bottom) at 60 kPa of stack pressure.

the 0 kPa condition for all pressures and both D_{max} and $D_{max/2}$. Holding pressure at a level value seemed to reduce discharge internal resistances, especially at SOCs below 70%. This coincides with the pulse pressure, as the CPF has a steeper pressure increase at SOCs above 70%. These benefits could come from effectively increasing surface area through pressure application, without excessively pressurising the cell. At Low SOCs, both the MBPF and CPF had the largest decreases in internal resistance compared to the 0 kPa test, indicating that applied stack pressure may have extra benefits at low SOCs. However, low SOCs are the point of the highest DCIR so the normalised difference in DCIR would indicate that the reduction in DCIR is proportional to the nominal value. The lesser difference in discharge DCIR above 70% SOC may be because DCIR is less dependent on pressure at high SOC. Both fixtures had fewer improvements in DCIR from the control condition at D_{max}. Between 30 and 60 kPa seemed optimal for both fixtures in terms of discharge resistance. 90 kPa may be excessively high for the MBPF, as the peak pressure reaching nearly 200 kPa could mitigate the benefits of pressure.

For the charge pulses (Fig. 7), the CPF generally had lower DCIR than the control condition for $D_{max/2}$, except for high SOCs where it had higher internal resistances. Both the CPF and MBPF had higher charge DCIR than the control condition for D_{max}. The MBPF had higher charge internal resistances at lower SOCs than the control condition but had similar charge internal resistances at higher SOCs. The CPF

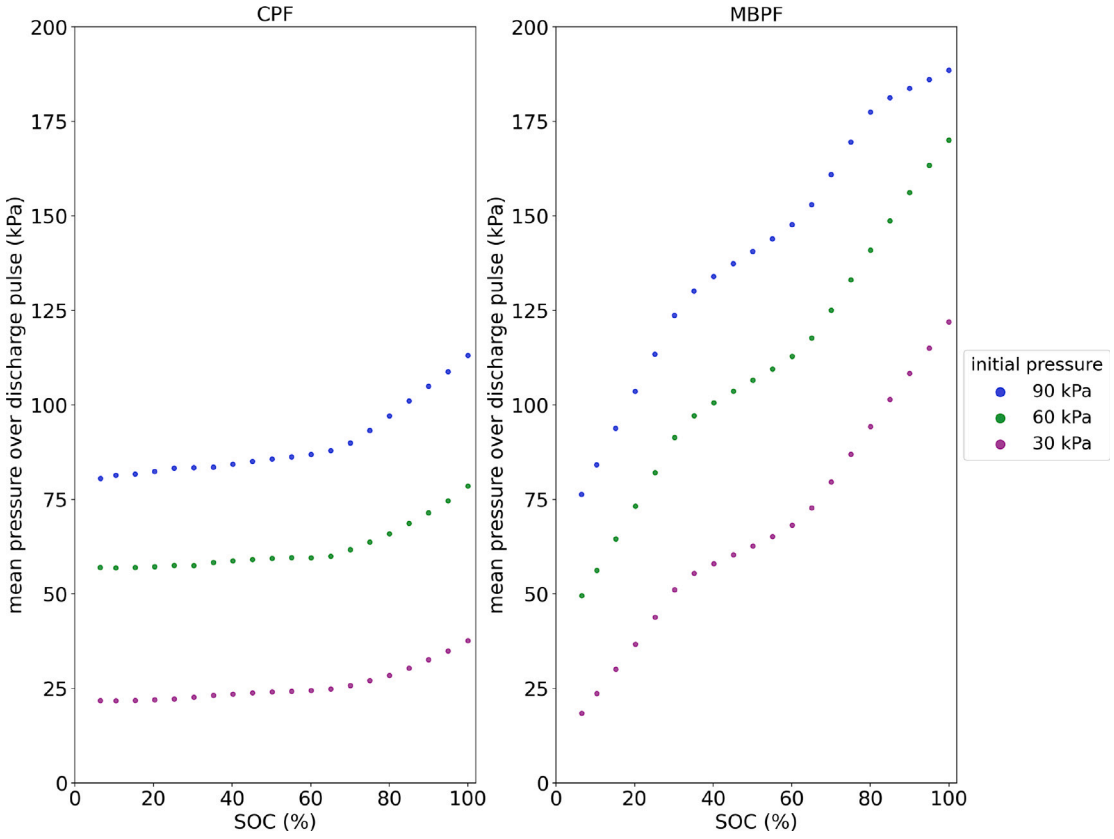

Fig. 5. The mean stack pressure for the 10 s discharge pulse for CPF (left) and MBPF (right) for three initial pressures across state-of-charge.

had a lower charge DCIR than the MBPF for nearly all cases, except high SOCs for $D_{max/2}$. Applied stack pressure could reduce charge performance, which is worse at higher C-rates. Similar to discharge DCIR, the 30 kPa and 60 kPa conditions seem more optimal than 90 kPa stack pressure. Pressure may negatively affect charge resistance due to the decrease in thickness with SOC due to the anode volume change. The applied pressure could be a driving force that biases discharge, as discharging the cell over time decreases thickness. For a 10-second pulse conducted in this study, it is difficult to evaluate if this effect explains the difference in discharge and charge resistance compared to having no stack pressure. The CPF at half the maximum current was the only beneficial condition for charge DCIR. Further investigation into this effect could reveal nuances of the effect of pressure on charge DCIR.

The maximum current D_{max} trial resulted in a lower charge and discharge DCIR for both fixtures and all pressures, including the control. The lower DCIR for the D_{max} current cycle could be due to the higher prescribed current changing the plating mechanisms of the electrode [37]. Higher current can accelerate electrochemical processes such as the double layer discharging quicker, reducing the DCIR [38]. This poses an interesting idea that higher current demands could reduce heat generation for pulse conditions in performance settings. This could explain the benefits of pulse charging at certain currents, where resistance is lower than steady charging, improving charging efficiency and fast charging times. The temperature was higher for the D_{max} condition because higher battery power results in higher heat generation. Since temperature only varied by 1 °C, it most likely did not affect the DCIR [37]. Both discharge and charge DCIR had maximum values at the lowest SOC point for all trials. Discharge DCIR values were generally lowest within the 30% to 60% SOC range, while charge DCIR values have a similar dip in the 30% to 60% range, with their lowest value near 100% SOC. DCIR increased at low SOC due to the reduction in available intercalation space in the cathode. Diffusion becomes more difficult as more lithium ions occupy available space in the cathode material, increasing resistance. Inversely, the charge DCIR increased at high SOC, due to the increased difficulty of intercalating lithium into the negative electrode. The charge DCIR had less of a resistance increase, which aligns with previous studies [39–41].

Power differences were also measured between the fixtures. Figs. 8 and 9 show the power plotted as a difference in discharge and charge power at various pressures compared to the control baseline, shown by the dashed line at $y = 0$. Generally, both the discharge and charge power increased with SOC, but the charge power was lowest at 95% SOC. Power increased with SOC due to the cell voltage vs SOC. Discharge power at low SOC and charge power at high SOC were both important metrics because minimum voltage and maximum voltage limit the power, respectively. At high SOCs, being able to keep cell voltage below the maximum cutoff voltage enables faster charging, while at low SOCs, maintaining a voltage above the minimum cut-off voltage enables higher discharge power. The CPF had higher discharge power than both the MBPF and control case for nearly all pressures and SOCs, except for 60 kPa of stack pressure. Increasing discharge current increased the difference in discharge power between the CPF and MBPF to the control condition. The CPF had greater power benefits at the higher current, while the MBPF had greater power detriments. The greater difference between the CPF and MBPF at D_{max} reveals that constant pressure could be more beneficial in terms of discharge power at high C-rates. The MBPF performed worse at higher C-rates, indicating that constraining displacement can be detrimental to cell performance in this scenario. The CPF had the largest increase of power at low SOCs, except for the 90 kPa condition. The CPF achieved a power

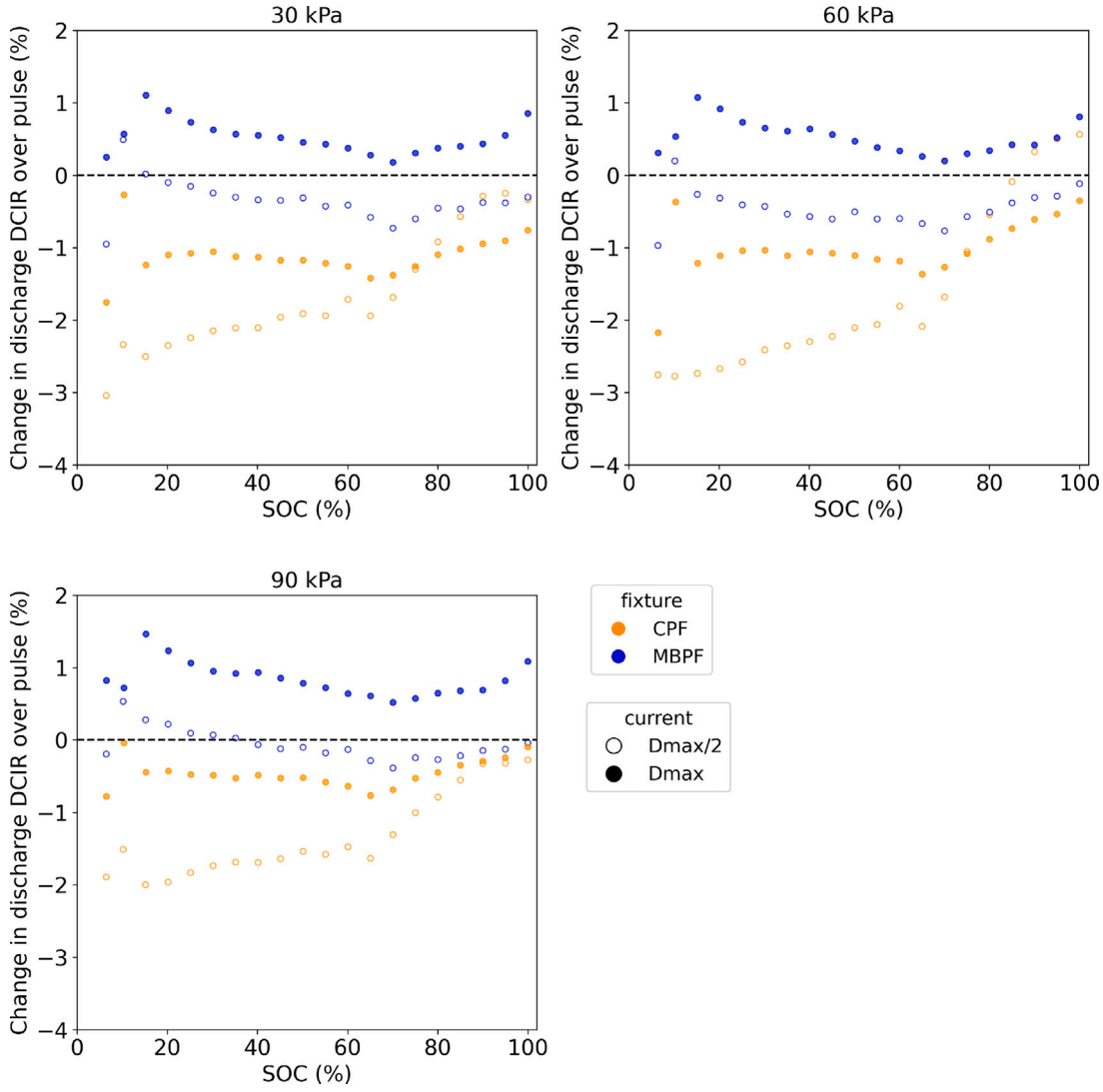

Fig. 6. Percent change in discharge DCIR vs SOC for the CPF and MBPF from the control condition at various initial pressures. Note for Figs. 6 and 7: The unconstrained control condition applies 0 kPa of pressure to the cell. The difference in DCIR between each of the two fixtures and the control condition are plotted at each SOC, with the control condition indicated with the dashed line.

difference on the last discharge pulse of 2.6% compared to 0 kPa and 4% compared to the MBPF when both fixtures were tested at 60 kPa. The CPF saw this smallest increase of power at 90 kPa, possibly due to pressure exceeding the limit of benefit for the cell. Similarly to DCIR, differences in charge power were less significant between the fixtures than discharge power. Both the CPF and MBPF had less charge power at high SOCs than the control condition, and slightly more charge power at low SOC. The loss of charge power at high SOC could be because of the previously mentioned idea that pressure can be adverse for charging in some cases. The MBPF had an edge over the CPF for charge power, especially at low SOCs for D_{max}. The CPF had less charge power than the control case for low SOCs at D_{max}, performing worst at 90 kPa.

Discharge capacity ranged from 3.84–3.86 Ah, for all fixtures constraints and for the control. Given that the differences in discharge capacity were less than 1%, there is not enough evidence to show that stack pressure affected discharge capacity in the short term. Lithium-ion pouch cells may not benefit from the capacity increase from stack pressure as with lithium-metal anode and silicon-blend anode cells, where much higher stack pressures showed improvements in capacity [19,26]. Hahn et al. [1] found that stack pressure decreased lithium-ion cell capacity initially, then provided better capacity retention during calendar ageing. The possible benefits of dendrite growth suppression, gas suppression, and SEI layer growth suppression would only emerge with degradation testing and/or calendar ageing.

4. Conclusion

A fixture was developed to evaluate the effects of constant pressure and constant displacement constraints on cell performance. The designed fixture performed as expected with pressure variations of below 25% when compared to a conventional fixed-displacement system with a pressure variation of over 300%. Improvements in discharge resistance and power were observed by applying constant pressure with no significant capacity or Coulombic efficiency differences were measured. Incorporating more uniform pressure on pouch cells independent of cell swelling could improve discharge capabilities for performance scenarios. Designing battery packs that pressurise pouch cells while allowing them to expand and contract could improve the discharge power of

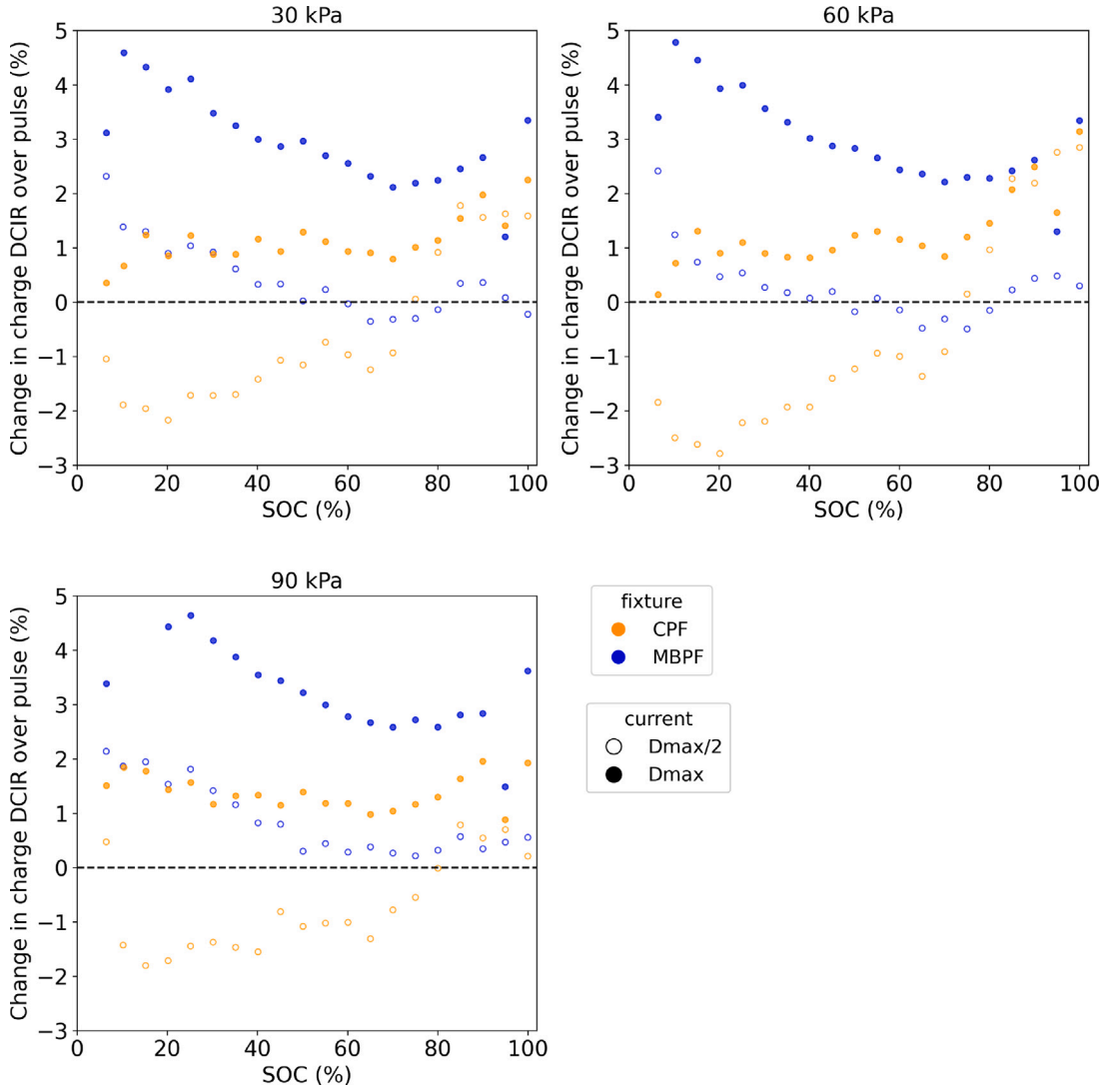

Fig. 7. Percent change in charge DCIR vs SOC for the CPF and MBPF from the control condition at various initial pressures.

packs, an important metric for performance scenarios. Additionally, lower discharge internal resistance would reduce power loss during discharge, improving vehicle performance.

Further work could reduce errors from sensors and mechanical flex to obtain higher fidelity data. The load cells measuring the pressure did have signal noise, although this was seen to be less than the change in pressures during the discharge and charge pulses. Nevertheless, hysteresis error and random error could have affected the pressure results. Incorporating a singular, more accurate load cell could improve the resolution and accuracy of the pressure data. Flexing in the pressure plates was seen during testing for both the CPF and MBPF, and was more noticeable at 90 kPa. This deformation could have negatively impacted pressure distribution, reducing the possible benefits of stack pressure. Selecting a different design for the plates in terms of materials or geometry could mitigate this possible source of error. Testing cell degradation with both fixtures could reveal possible long-term capacity benefits from applying constant stack pressure.

CRediT authorship contribution statement

Aiden Leonard: Conceptualization, Methodology, Software, Formal analysis, Investigation, Writing – original draft, Writing – review & editing, Visualization. **Brady Planden:** Conceptualization, Software, Resources, Writing – review & editing, Supervision, Project administration. **Katie Lukow:** Conceptualization, Software, Resources, Writing – review & editing, Supervision, Project administration. **Denise Morrey:** Resources, Supervision, Project administration, Funding acquisition.

Declaration of competing interest

The authors declare that they have no known competing financial interests or personal relationships that could have appeared to influence the work reported in this paper.

Data availability

For questions in regard to obtaining test data, please contact the High Voltage Energy Storage group at Oxford Brookes University: https://www.brookes.ac.uk/research/units/tde/groups/high-voltage-and-energy-storage.

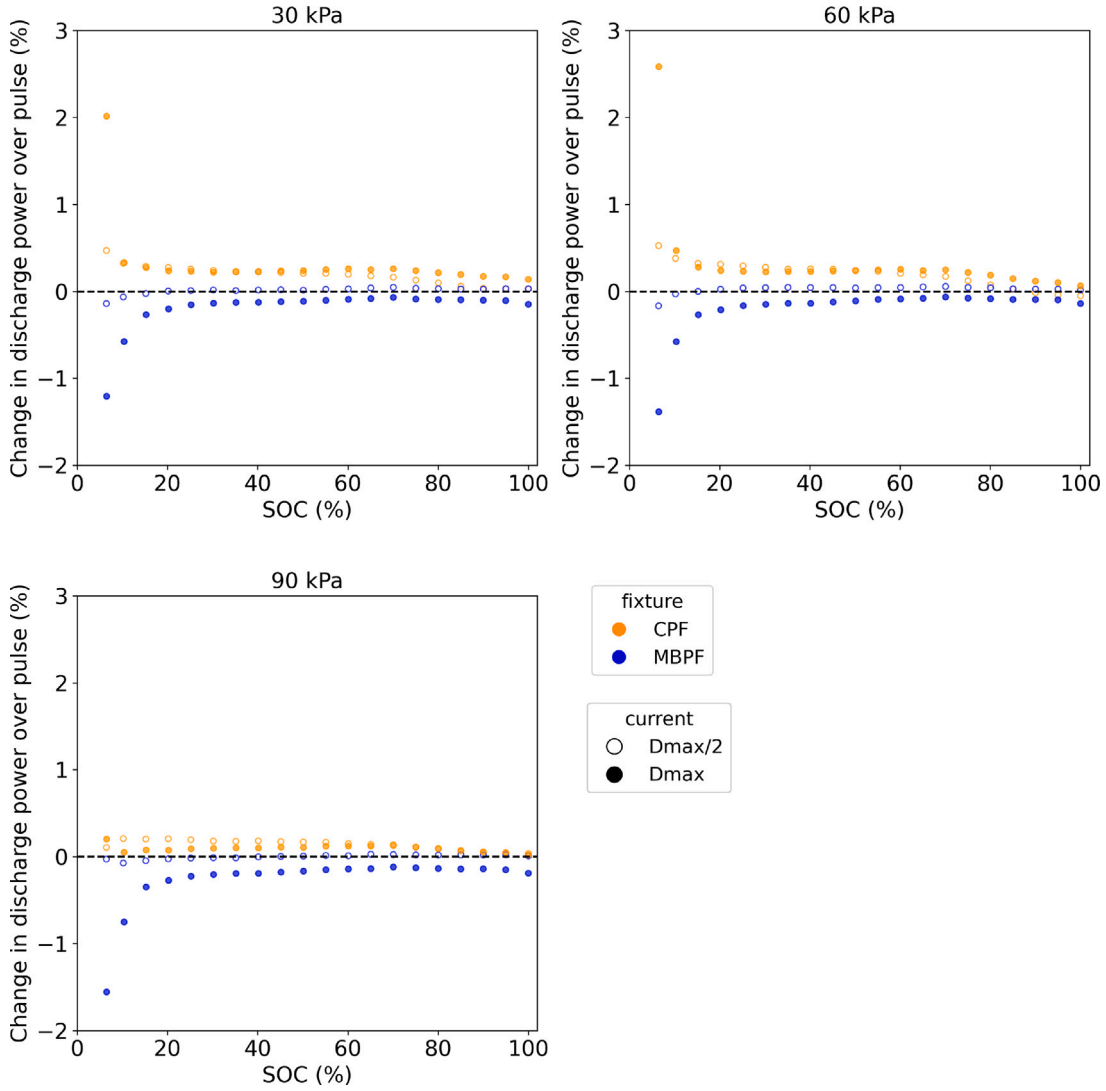

Fig. 8. Percent change in discharge power vs SOC for the CPF and MBPF from the control condition at various initial pressures. Note for Figs. 8 and 9: The unconstrained control condition applies 0 kPa of pressure to the cell. The difference in power between each of the two fixtures and the control condition are plotted at each SOC, with the control condition indicated with the dashed line.

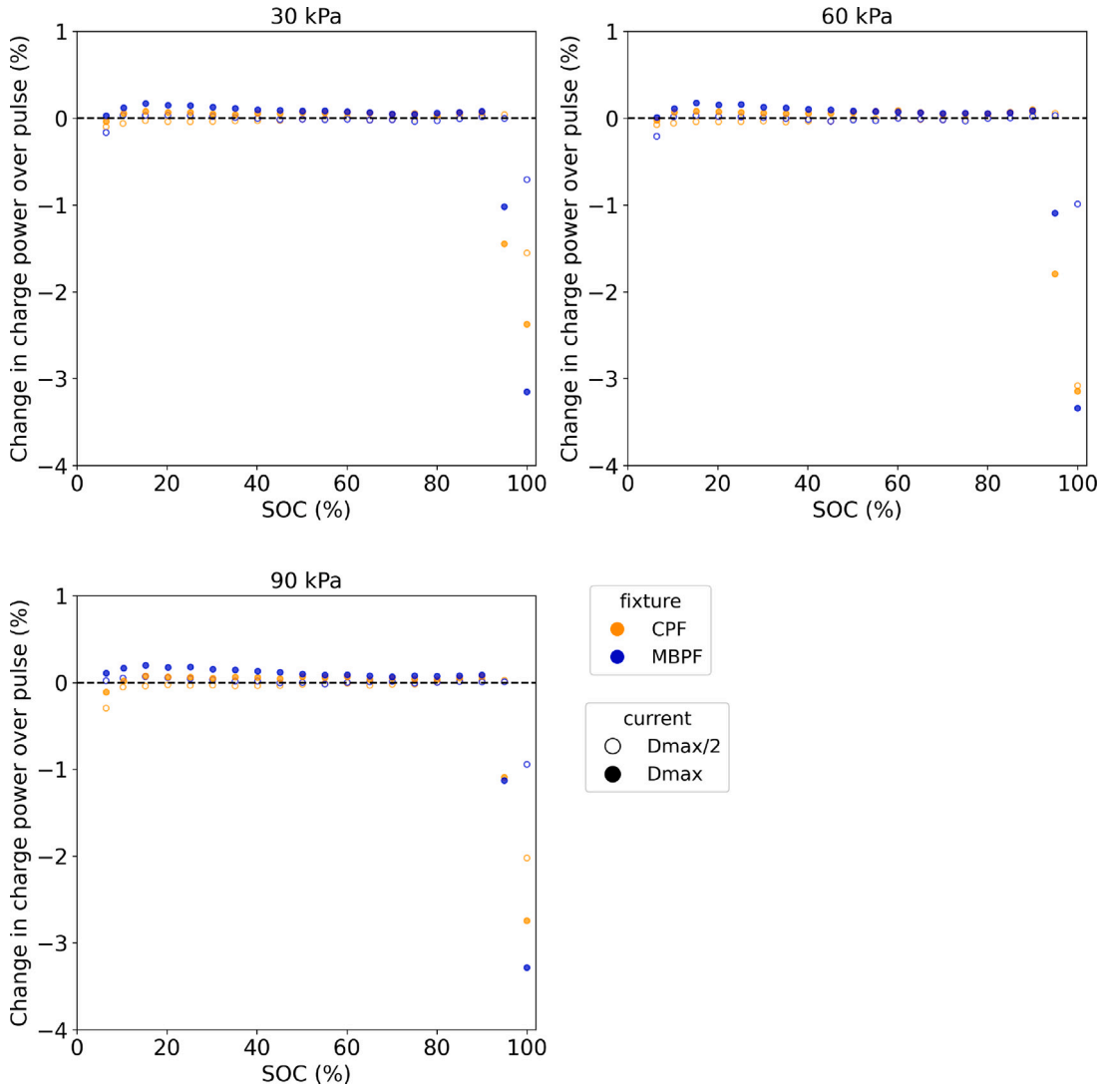

Fig. 9. Percent change in charge power vs SOC for the CPF and MBPF from the control condition at various initial pressures.

References

[1] Severin Hahn, et al., Pressure prediction modeling and validation for lithium-ion pouch cells in buffered module assemblies, J. Energy Storage 40 (2021) 102517, http://dx.doi.org/10.1016/j.est.2021.102517, URL https://www.sciencedirect.com/science/article/pii/S2352152X21002656.

[2] Yihui Jiang, et al., A stack pressure based equivalent mechanical model of lithium-ion pouch batteries, Energy 221 (2021) 119804, http://dx.doi.org/10.1016/j.energy.2021.119804, URL https://www.sciencedirect.com/science/article/pii/S0360544221000530.

[3] Abdilbari Shifa Mussa, et al., Effects of external pressure on the performance and ageing of single-layer lithium-ion pouch cells, J. Power Sources 385 (2018) 18–26, http://dx.doi.org/10.1016/j.jpowsour.2018.03.020, URL https://linkinghub.elsevier.com/retrieve/pii/S0378775318302441.

[4] Long Zhou, et al., A study of external surface pressure effects on the properties for lithium-ion pouch cells, Int. J. Energy Res. 44 (8) (2020) 6778–6791.

[5] Verena Müller, et al., Study of the influence of mechanical pressure on the performance and aging of Lithium-ion battery cells, J. Power Sources 440 (2019) 227148, http://dx.doi.org/10.1016/j.jpowsour.2019.227148.

[6] Ruihe Li, et al., Effect of external pressure and internal stress on battery performance and lifespan, Energy Storage Mater. 52 (2022) 395–429, http://dx.doi.org/10.1016/j.ensm.2022.07.034, URL https://www.sciencedirect.com/science/article/pii/S2405829722004044.

[7] John Cannarella, Craig B. Arnold, Stress evolution and capacity fade in constrained lithium-ion pouch cells, J. Power Sources 245 (2014) 745–751, http://dx.doi.org/10.1016/j.jpowsour.2013.06.165, URL https://www.sciencedirect.com/science/article/pii/S037877531301197X.

[8] Christina Peabody, Craig B. Arnold, The role of mechanically induced separator creep in lithium-ion battery capacity fade, J. Power Sources 196 (19) (2011) 8147–8153, http://dx.doi.org/10.1016/j.jpowsour.2011.05.023, URL https://www.sciencedirect.com/science/article/pii/S037877531100989X.

[9] Shaojun Niu, et al., Analysis on the effect of external press force on the performance of LiNi0.8Co0.1Mn0.1O2/Graphite large pouch cells, J. Energy Storage 44 (2021) 103425, http://dx.doi.org/10.1016/j.est.2021.103425, URL https://www.sciencedirect.com/science/article/pii/S2352152X21011117.

[10] John Cannarella, Craig B. Arnold, State of health and charge measurements in lithium-ion batteries using mechanical stress, J. Power Sources 269 (2014) 7–14, http://dx.doi.org/10.1016/j.jpowsour.2014.07.003, URL https://www.sciencedirect.com/science/article/pii/S0378775314010453.

[11] A.J. Louli, L.D. Ellis, J.R. Dahn, Operando pressure measurements reveal solid electrolyte interphase growth to rank Li-ion cell performance, Joule 3 (3) (2019) 745–761.

[12] Emanuele Michelini, et al., Experimental investigation on reversible swelling mechanisms of lithium-ion batteries under a varying preload force, Batteries 9 (4) (2023) http://dx.doi.org/10.3390/batteries9040218, URL https://www.mdpi.com/2313-0105/9/4/218.

[13] Jean-Marie Doux, et al., Pressure effects on sulfide electrolytes for all solid-state batteries, J. Mater. Chem. A 8 (2020) 5049–5055, http://dx.doi.org/10.1039/C9TA12889A.

[14] Wesley Chang, et al., Evolving contact mechanics and microstructure formation dynamics of the lithium metal-Li7La3Zr2O12 interface, Nature Commun. 12 (2021) 6369, http://dx.doi.org/10.1038/s41467-021-26632-x.

[15] Xin Zhang, et al., Pressure-driven interface evolution in solid-state lithium metal batteries, Cell Rep. Phys. Sci. 1 (2) (2020) 100012, http://dx.doi.org/10.1016/j.xcrp.2019.100012, URL https://www.sciencedirect.com/science/article/pii/S266638641930013X.

[16] Alexander J. Louli, et al., Exploring the impact of mechanical pressure on the performance of anode-free lithium metal cells, J. Electrochem. Soc. 166 (8) (2019) A1291–A1299.
[17] Cameron Martin, et al., Cycling lithium metal on graphite to form hybrid lithium-ion/lithium metal cells, Joule 4 (2020) 1296–1310, http://dx.doi.org/10.1016/j.joule.2020.04.003.
[18] Gregory L. Plett, Battery Management Systems. Volume I, Battery Modeling, 2015.
[19] Gert Berckmans, et al., Electrical characterization and micro X-ray computed tomography analysis of next-generation silicon alloy lithium-ion cells, World Electr. Veh. J. 9 (3) (2018) 43, http://dx.doi.org/10.3390/wevj9030043, https://www.mdpi.com/2032-6653/9/3/43.
[20] Charles Monroe, John Newman, The effect of interfacial deformation on electrodeposition kinetics, J. Electrochem. Soc. 151 (2004) A880–A886, http://dx.doi.org/10.1149/1.1710893.
[21] Sangil Hyun, Mark O. Robbins, Elastic contact between rough surfaces: Effect of roughness at large and small wavelengths, Tribol. Int. 40 (10) (2007) 1413–1422, http://dx.doi.org/10.1016/j.triboint.2007.02.003, Tribology at the Interface: Proceedings of the 33rd Leeds-Lyon Symposium on Tribology (Leeds, 2006), URL https://www.sciencedirect.com/science/article/pii/S0301679X07000369.
[22] Joachim Larsson, Shiro Biwa, Bertil Storåkers, Inelastic flattening of rough surfaces, Mech. Mater. 31 (1) (1999) 29–41, http://dx.doi.org/10.1016/S0167-6636(98)00046-5, URL https://www.sciencedirect.com/science/article/pii/S0167663698000465.
[23] H.M. Stanley, T. Kato, An FFT-based method for rough surface contact, J. Tribol. 119 (3) (1997) 481–485, http://dx.doi.org/10.1115/1.2833523, arXiv:https://asmedigitalcollection.asme.org/tribology/article-pdf/119/3/481/5602831/481_1.pdf.
[24] Shashank Arora, Weixiang Shen, Ajay Kapoor, Review of mechanical design and strategic placement technique of a robust battery pack for electric vehicles, Renew. Sustain. Energy Rev. 60 (2016) 1319–1331, http://dx.doi.org/10.1016/j.rser.2016.03.013, URL https://www.sciencedirect.com/science/article/pii/S1364032116002483.
[25] Lip Huat Saw, Yonghuang Ye, Andrew A.O. Tay, Integration issues of lithium-ion battery into electric vehicles battery pack, J. Clean. Prod. 113 (2016) 1032–1045, http://dx.doi.org/10.1016/j.jclepro.2015.11.011, URL https://www.sciencedirect.com/science/article/pii/S0959652615016406.
[26] Gert Berckmans, et al., Analysis of the effect of applying external mechanical pressure on next generation silicon alloy lithium-ion cells, Electrochim. Acta 306 (2019) 387–395, http://dx.doi.org/10.1016/j.electacta.2019.03.138, URL https://www.sciencedirect.com/science/article/pii/S0013468619305614.
[27] Lysander De Sutter, et al., Mechanical behavior of silicon-graphite pouch cells under external compressive load: Implications and opportunities for battery pack design, J. Power Sources 451 (2020) 227774, http://dx.doi.org/10.1016/j.jpowsour.2020.227774, URL https://www.sciencedirect.com/science/article/pii/S037877532030077X.
[28] Bernhard Bitzer, Andreas Gruhle, A new method for detecting lithium plating by measuring the cell thickness, J. Power Sources 262 (2014) 297–302, http://dx.doi.org/10.1016/j.jpowsour.2014.03.142, URL https://www.sciencedirect.com/science/article/pii/S0378775314004753.
[29] Davide Clerici, Francesco Mocera, Aurelio Somà, Electrochemical–mechanical multi-scale model and validation with thickness change measurements in prismatic lithium-ion batteries, J. Power Sources 542 (2022) 231735, http://dx.doi.org/10.1016/j.jpowsour.2022.231735, URL https://www.sciencedirect.com/science/article/pii/S0378775322007297.
[30] B. Rieger, et al., Multi-scale investigation of thickness changes in a commercial pouch type lithium-ion battery, J. Energy Storage 6 (2016) 213–221, http://dx.doi.org/10.1016/j.est.2016.01.006, URL https://www.sciencedirect.com/science/article/pii/S2352152X16300068.
[31] Katie Lukow, MBPF, 2022, http://dx.doi.org/10.5281/zenodo.7509368, URL https://github.com/katielukow/MBPF.
[32] High Voltage Energy Storage Group, Battery Testing Consortium Protocol, 2022, URL https://github.com/HVES-Battery-Testing-Consortium/LG-HG2.
[33] V.G. Choudhari, Dr A.S. Dhoble, T.M. Sathe, A review on effect of heat generation and various thermal management systems for lithium ion battery used for electric vehicle, J. Energy Storage 32 (2020) 101729, http://dx.doi.org/10.1016/j.est.2020.101729, URL https://www.sciencedirect.com/science/article/pii/S2352152X20315668.
[34] Yongqi Xie, et al., Experimental and analytical study on heat generation characteristics of a lithium-ion power battery, Int. J. Heat Mass Transfer 122 (2018) 884–894, http://dx.doi.org/10.1016/j.ijheatmasstransfer.2018.02.038, URL https://www.sciencedirect.com/science/article/pii/S001793101733421X.
[35] Ki-Yong Oh, Bogdan I. Epureanu, A novel thermal swelling model for a rechargeable lithium-ion battery cell, J. Power Sources 303 (2016) 86–96, http://dx.doi.org/10.1016/j.jpowsour.2015.10.085, URL https://www.sciencedirect.com/science/article/pii/S0378775315304730.
[36] Yan Zhao, et al., Localized swelling inhomogeneity detection in lithium ion cells using multi-dimensional laser scanning, J. Electrochem. Soc. 166 (2) (2019) A27.
[37] Anup Barai, et al., A study of the influence of measurement timescale on internal resistance characterisation methodologies for lithium-ion cells, Sci. Rep. 8 (1) (2018) 1–13.
[38] Wladislaw Waag, Stefan Käbitz, Dirk Uwe Sauer, Experimental investigation of the lithium-ion battery impedance characteristic at various conditions and aging states and its influence on the application, Appl. Energy 102 (2013) 885–897, http://dx.doi.org/10.1016/j.apenergy.2012.09.030, Special Issue on Advances in sustainable biofuel production and use - XIX International Symposium on Alcohol Fuels - ISAF, URL https://www.sciencedirect.com/science/article/pii/S030626191200671X.
[39] Tobias Teufl, et al., State of charge dependent resistance build-up in Li-and Mn-rich layered oxides during lithium extraction and insertion, J. Electrochem. Soc. 166 (6) (2019) A1275.
[40] Jianming Zheng, et al., Electrochemical kinetics and performance of layered composite cathode material Li [Li0. 2Ni0. 2Mn0. 6] O2, J. Electrochem. Soc. 160 (11) (2013) A2212.
[41] Sanketh R. Gowda, et al., Examining the electrochemical impedance at low states of charge in lithium-and manganese-rich layered transition-metal oxide electrodes, J. Electrochem. Soc. 162 (7) (2015) A1374.